

SAMPLING CONDITIONED DIFFUSIONS VIA PATHSPACE PROJECTED MONTE CARLO

ABSTRACT. We present an algorithm to sample stochastic differential equations conditioned on rather general constraints, including integral constraints, endpoint constraints, and stochastic integral constraints. The algorithm is a pathspace Metropolis-adjusted manifold sampling scheme, which samples stochastic paths on the submanifold of realizations that adhere to the conditioning constraint. We demonstrate the effectiveness of the algorithm by sampling a dynamical condensation phase transition, conditioning a random walk on a fixed Levy stochastic area, conditioning a stochastic nonlinear wave equation on high amplitude waves, and sampling a stochastic partial differential equation model of turbulent pipe flow conditioned on relaminarization events.

1. BACKGROUND

Stochastic differential equations form the basis of a multitude of models in the sciences: The degrees of freedom under consideration evolve according to a known and deterministic model, and all uncertainty or unresolved processes can be added as stochasticity. In many cases of interest, one is then interested in the probability distribution of observables of the model conditional on some physically meaningful event. Examples include teleconnection patterns during heat waves [1, 2], the pathway to the collapse of the Atlantic meridional overturning circulation [3, 4] or other climate tipping points [5], the probability of large “rogue” waves in the ocean [6, 7], or the expected waiting time for rare events in fluids, such as the proliferation of turbulence in pipe flow [8, 9], or the rupture of a liquid nanofilm [10–12]. In all these cases, we are interested in drawing realizations of the stochastic process, but conditioned on a particular outcome. This problem is most difficult if the particular outcome is *rare* (as in all examples above), such that naively sampling the process many times will yield almost no realizations of the constraint, and thus any conditional statistics are very hard to obtain.

The answer to this problem are specifically crafted *rare event algorithms*. This contains methods to directly bias the dynamics to observe certain rare events (which falls under the class of importance sampling Monte Carlo algorithms), or alternatively *effectively* bias an ensemble of simulations by subselection, cloning, and pruning (also known as importance splitting, such as sequential Monte-Carlo, multilevel splitting [13], or genealogical particle algorithms [14]). Opposed to this are sampling free rare events methods, for example based on large deviation theory, to estimate rare events by their most likely singular occurrence [15]. Lastly, one can directly draw from the dynamics conditioned on the rare outcome, which includes theoretical tools like the Doob transform [16], as well as numerical methods such as transition path sampling [17–19] and bridge sampling [20–23]. Here, we will consider an algorithm of the latter class, but not only for bridges, or transitions from one point in the state space to another, but on rather arbitrary observables, including time-integrated ones, those that are the result of stochastic integrals along the process, or observables that are a nonlinear function of the final realized configuration after a random temporal evolution.

The algorithm falls into the class of Metropolis-adjusted pathspace Monte Carlo samplers [20, 24–27], but realized on manifolds, where the manifold is the set of random parameters that realize the constraint. While we restrict it here to additive and multiplicative Gaussian stochastic (partial) differential equations, the generalization to arbitrary stochastic processes with random parameters is straightforward.

For this, we will introduce our considered setup in section 2. Then, in section 3 we will present our algorithm, by first discussing existing pathspace sampling and diffusion bridge sampling ideas in section 3.1, and then developing our algorithm in sections 3.2 to 3.5. Following that, in section 4, we will demonstrate the applicability of the algorithm to various problems, namely range statistics of the standard Brownian bridge in section 4.1, a dynamical condensation phase transition in section 4.2, the stochastic Levy area in section 4.3, a PDE case of large waves in the nonlinear Korteweg-deVries wave equation in section 4.4, and lastly the decay of turbulent puffs in a model of subcritical pipe flow in section 4.5. We close off with a discussion in section 5. Some issues and open questions for the scalability of the algorithm in infinite dimensional Wiener space is discussed in appendix A.

2. SETUP

Consider the (additive Gaussian) SDE for X_t on \mathbb{R}^n with $t \in [0, T]$ given by

$$dX_t = b(X_t) dt + \sigma dW_t, \quad X_0 = x_0, \quad (1)$$

for some drift vector field $b : \mathbb{R}^n \rightarrow \mathbb{R}^n$, and diffusion matrix $\sigma \in \mathbb{R}^{n \times m}$, with W_t being m -dimensional Brownian motion. For notational purposes, we define the ordinary differential equation

$$\dot{\phi}(t) = b(\phi) + \sigma \eta \quad (2)$$

for $\phi : [0, T] \rightarrow \mathbb{R}^n$ that maps some noise realization $\eta \in L^2([0, T], \mathbb{R}^m)$ to an outcome trajectory, and associate it with the solution map $\Phi : \eta \mapsto \phi$. Then, we define as $f(\phi) : L^2([0, T], \mathbb{R}^n) \rightarrow \mathbb{R}$ the *observable* that maps a trajectory to our desired outcome (for example measuring properties of the final configuration $\phi(T)$, or some integral constraint of $\int_0^T g(\phi(t)) dt$). Similarly, the *noise-to-event* map $F = f \circ \Phi$ maps a noise realization directly to the outcome, through the implicit integration of the underlying differential equation. We then want to condition the process so that the observable takes a certain value $F(\eta) = f(\Phi(\eta)) = z \in \mathbb{R}$. In other words, we want to restrict ourselves only to noise realizations $\eta \in L^2([0, T], \mathbb{R}^m)$ that realize a given value $z \in \mathbb{R}$ under the process (1).

While we could consider conditioning on more than a scalar variable, i.e. $z \in \mathbb{R}^d$, we will restrict ourselves to the scalar case for ease of notation. The vectorial case is conceptually the same. Similarly, we could (and in fact will, for example in section 4.3) consider multiplicative Gaussian noise, by taking a $\sigma(X_t)$ dependent on the state X_t of the process, which leads to some additional terms further on, but is, again, conceptually the same.

3. PATHSPACE METROPOLIS-HASTINGS ON CONDITIONED SUBSET

The goal is now to *sample* the process (1) conditioned on the outcome z , i.e. drawing trajectories $\phi(t)$ solution to (2) with $f(\phi) = z$, but with correct weights, in that more likely ways to realize the constraint should be preferred over less likely ones. This will yield an *ensemble* of conditioned trajectories, which is helpful for analyzing physical mechanisms that are responsible for realizing the given observable. For example, conditioning a nonlinear wave equation on a high wave at some final time, we might be interested in investigating *how* such large waves are produced by drawing many samples of them and investigating their common features. If the event is rare, this might otherwise be prohibitively expensive to do. Being able to sample the conditioned process is even more important when considering obtaining conditioned probabilities or probability distributions in complicated physical processes. For example, for a weather model, one might be interested in the probability distribution of wind speeds at a given location, conditional on there being anomalously high cloud cover for a long duration, for the purposes of estimating necessary energy storage capacities for renewable energy.

3.1. Bridge Sampling and Pathspace Langevin MCMC. A special case is the situation where we choose $f(\phi) = \phi(T)$, i.e. where the observable of interest is the endpoint itself. Since the state space is \mathbb{R}^n , this is a conditioning on more than a scalar constraint if $n > 1$, but related to our setup. In particular, this is the case of *diffusion bridge sampling* or *transition path sampling*.

We first discuss the case where the diffusion vector field is gradient, $b(x) = -\nabla V(x)$, for a potential $V : \mathbb{R}^n \rightarrow \mathbb{R}$, which is of considerable interest in for example molecular dynamics, where one is interested in a *reaction* as sample path connecting two local minima of a free energy landscape. Then, simplifications apply, such that transition path sampling can be implemented very efficiently. The reason for that is first that knowledge of the potential landscape implies knowledge of the invariant measure of the process, and second that gradient dynamics correspond to a *reversible* Markov process, such that the time-reversed dynamics can feasibly be integrated as well. As such, transition paths fulfill time-reversibility constraints, which allow for more effective sampling [17, 18, 28].

In the non-reversible setup, i.e. for arbitrary vector fields $b : \mathbb{R}^n \rightarrow \mathbb{R}^n$, the situation is less straightforward. Still, in general, we know that the Onsager-Machlup functional

$$S_{\text{OM}}(\phi) = \frac{1}{2} \int_0^T (\|\dot{\phi} - b(\phi)\|_{\sigma}^2 + \nabla \cdot b(\phi)) dt$$

(for a specific σ -dependent norm $\|v\|_{\sigma} = (v \cdot (\sigma \sigma^{\top})^{-1} v)^{1/2}$) quantifies a formal ‘‘density’’ in pathspace of sample paths of the process (1), or in other words, the pathspace measure formally fulfills $d\mathbb{P}(\phi) \sim e^{-S_{\text{OM}}(\phi)} d\phi$.

Therefore, we can build a Langevin MCMC algorithm by constructing a Markov chain with invariant measure proportional to $e^{-S_{\text{OM}}}$, which is given for example by the pathspace Langevin equation in virtual (‘‘algorithmic’’)

time τ given by

$$\partial_\tau \phi(t, \tau) = -\frac{\delta S_{\text{OM}}(\phi)}{\delta \phi} + \xi(t, \tau), \quad (3)$$

where $\mathbb{E}\xi\xi^t = \delta(t-t')\delta(\tau-\tau')$ is white-in-time and virtual time. When expanding the variational derivative of the Onsager-Machlup action, the SPDE (3) for $\phi(t, \tau) : [0, T] \times \mathbb{R}^+ \rightarrow \mathbb{R}^n$, then becomes,

$$\partial_\tau \phi = (\sigma\sigma^\top)^{-1} \partial_{tt} \phi - (\sigma\sigma^\top)^{-1} \nabla b(\phi) - \nabla b(\phi)^\top (\sigma\sigma^\top)^{-1} - b(\phi) \nabla b(\phi) - \nabla(\nabla \cdot b(\phi)) + \xi(t, \tau) \quad (4)$$

equipped with boundary conditions

$$\phi(0, \tau) = x_0 \quad \text{and} \quad \phi(T, \tau) = z. \quad (5)$$

The SPDE (4) has as unique invariant measure (in pathspace) the bridge measure of (1) conditioned on $\phi(T) = z$. While these arguments are rather formal, they can be made rigorous for a variety of cases [20, 26, 27], though notably still appear to be open for arbitrary vector fields b (since then the SPDE (4) might become singular). This pathspace Langevin MCMC sampler can even be imbued with metadynamics [29] to sample in the case of multiple coexistent transition channels [19].

Unfortunately, constraints different from mere endpoint constraints can no longer be implemented in the form of (3) in an easy way: We would need to draw new paths ϕ according to more complicated restrictions, for example on whole integrals of the trajectory, which are not simply encoded in a physical-time boundary condition as in (5). The same complications arise if σ is not invertible, which is generally true if $m < n$, as (4) relies on the existence of $(\sigma\sigma^\top)^{-1}$. This case, sometimes called the *degenerate* or *hypoelliptic* case, is often relevant in practical application as not all degrees of freedom of a physical system are presumed to be uncertain or random. The fact that in this case the bridge sampling fails is rather intuitive, since it just means that the noise-to-path map $\Phi(\eta)$ is not invertible (in that there are paths ϕ that cannot be realized by any choice of noise η). In this case, one would rather want to draw random noise realizations (which are only conditioned on a specific observable outcome) as opposed to random trajectory realizations (which must be realizable by the noise). This is indeed the direction that we will follow here.

3.2. Conditioned sampling as sampling on a manifold. Instead, we might consider sampling not for trajectory realizations ϕ , but employing the same idea for noise realizations η . Formally, we can consider $\eta \sim dW/dt$ in (2), i.e. consider a measure μ on the space of trajectories that scales like

$$d\mu(\eta) \propto \exp\left(-\frac{1}{2} \int_0^T |\eta(t)|^2 dt\right) d\eta = \exp\left(-\frac{1}{2} \|\eta\|^2\right) d\eta = p(\eta), \quad (6)$$

where the norm $\|\cdot\|$ is $L^2([0, T], \mathbb{R}^m)$ (this intuitive notion can be made precise via the classical Wiener space, as we discuss in appendix A). While it is not difficult to draw noise realizations η , the problem is that almost surely a random η will not fulfill our constraint $F(\eta) = z$. For this reason, the main idea we consider here is to define a manifold in the space of noise realizations

$$\mathcal{M}_z = \{\eta \in L^2([0, T], \mathbb{R}^m) \mid F(\eta) = z\} \subset L^2([0, T], \mathbb{R}^m),$$

consisting of noise realizations that fulfill the global constraint on $\Phi(\eta)$ (i.e. $\mathcal{M}_z = F^{-1}(\{z\})$). In other words, we want to sample a Gaussian random variable on a submanifold. This can be achieved by drawing noise realizations under the constraint for example via an MCMC with an update step and subsequent projection onto \mathcal{M}_z .

Zappa *et al.* [30] specify a scheme to sample a probability measure known up to normalization constant, but constrained onto a submanifold of Euclidean space (see also [31–34] for sampling on submanifolds, and [35] for solving differential equations on constraint manifolds). The main idea is to construct a Metropolis adjusted Markov chain Monte Carlo on manifolds by a careful (and statistically reversible) projection procedure. Concretely, given a point $x \in \mathcal{M}_z$, we find a new point $y \in \mathcal{M}_z$ by the following steps:

- (i) Find the tangent space $T_x \mathcal{M}_z$.
- (ii) Draw a random element $v \in T_x \mathcal{M}_z$ from this tangent space, for example normally distributed.
- (iii) In general, $x + v \notin \mathcal{M}_z$, and we need to project back onto \mathcal{M}_z . This is done by finding a $w \perp T_x \mathcal{M}_z$ such that $x + v + w = y \in \mathcal{M}_z$.
- (iv) Accept or reject y based on a Metropolis Hastings rejection step to achieve the desired target distribution.

We argue here that the above remains not only valid, but numerically practical, when applied to whole trajectories, i.e. to sampling noise realizations $\eta \in L^2([0, T], \mathbb{R}^m)$ defining trajectories of stochastic differential equations, constrained to a manifold that realizes a scalar constraint $F(\eta) = z$. In the following, we will discuss the above steps in light of this generalization.

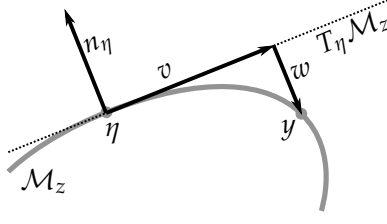


FIGURE 1. Sketch of the submanifold sampling technique. Given a point $\eta \in \mathcal{M}_z$, and a random $v \in T_\eta \mathcal{M}_z$, find $w \perp T_\eta \mathcal{M}_z$ such that $y = \eta + v + w \in \mathcal{M}_z$. Lastly, the proposal y is accepted via a Metropolis-Hastings rejection step.

3.3. Finding the tangent space. In order to find the tangent space $T_\eta \mathcal{M}_z$ at a given noise realization η , we require the computation of the gradient of the noise-to-observable map $F = f \circ \Phi$. Given that F implicitly necessitates the solution of an ODE and gradients are potentially high dimensional, care must be taken to compute it in a scalable way. We can apply the adjoint formalism (following for example [36]) to our problem of computing the normal vector to \mathcal{M}_z at a point $\eta \in L^2([0, T], \mathbb{R}^m)$. To do so, define the forward equation implicitly by constructing a residual map $\Psi : L^2([0, T], \mathbb{R}^n) \times L^2([0, T], \mathbb{R}^m) \rightarrow L^2([0, T], \mathbb{R}^n)$ with

$$\Psi(\phi, \eta) = \partial_t \phi - b(\phi) - \sigma \eta$$

so that $\Psi(\phi, \eta) = 0$ whenever the trajectory and noise pair (ϕ, η) fulfill our original SDE. Then, we can set

$$\frac{\delta F}{\delta \eta} = \left(\frac{\delta \Psi}{\delta \eta} \right)^\top \mu \quad \text{where } \mu \text{ is given by } \quad \left(\frac{\delta \psi}{\delta \phi} \right)^\top \mu = \frac{\delta f}{\delta \phi}.$$

In particular, it is clear that

$$\frac{\delta \Psi}{\delta \phi} = \partial_t - \nabla b(\phi) \quad \text{and} \quad \frac{\delta \Psi}{\delta \eta} = \sigma,$$

so that we have $\frac{\delta F}{\delta \eta} = \sigma^\top \mu$ where μ solves the differential equation

$$\partial_t \mu = -\nabla b(\phi)^\top \mu - \frac{\delta f}{\delta \phi}. \quad (7)$$

Equation (7) is the *adjoint equation* to the forward equation (2). We have now found the normal vector at η to \mathcal{M}_z : It is the vector $n_\eta = \sigma^\top \mu \in L^2([0, T], \mathbb{R}^m)$ obtained by solving the adjoint equation (7). Even though we need to keep in mind that η is not differentiable in time, and so care must be taken to define the proper derivative in terms of stochastic analysis (compare appendix A.4), ultimately the finite dimensional truncation remains the same.

This also allows us to project onto the tangent space $T_\eta \mathcal{M}_z$ of \mathcal{M}_z at location η via the orthogonal projection operator

$$\Pi_{T_\eta \mathcal{M}_z} v = v - \frac{\langle n_\eta, v \rangle}{\langle n_\eta, n_\eta \rangle} n_\eta,$$

where the inner product $\langle \cdot, \cdot \rangle$ is in $L^2([0, T], \mathbb{R}^m)$. This projection operator can be used to generate proposed update vectors $v \in T_\eta \mathcal{M}_z$, for example by drawing a normally distributed vector, and applying $\Pi_{T_\eta \mathcal{M}_z}$ to it. We now want to discuss a few special cases of observables.

3.3.1. Endpoint constraints. Often, we want a constraint on the endpoint, i.e. we want to constrain the final point X_T for the SDE (1) to be equal to a value $z \in \mathbb{R}$. This is the case of the stochastic bridge. In this case, the observable $f(\phi) = g(\phi(T))$, so that formally $\frac{\delta f}{\delta \phi} = \delta(t-T)(\nabla g(\phi(T)))$. This then yields a *boundary condition* for the adjoint equation (7), i.e.

$$\partial_t \mu = -\nabla b(\phi)^\top \mu, \quad \mu(T) = -\nabla g(\phi(T)).$$

3.3.2. Integral constraints. Instead, we might want to have an integral constraint, i.e. $f(\phi) = \int_0^T g(\phi(t)) dt$. In that case, $\frac{\delta f}{\delta \phi} = \nabla g(\phi(t))$, which yields a source term for the adjoint equation,

$$\partial_t \mu = -\nabla b(\phi)^\top \mu - \nabla g(\phi(t)), \quad \mu(T) = 0.$$

3.4. Backprojection onto the submanifold. Once a $v \in T_\eta \mathcal{M}_z$ is found, of course in general $\eta + v \notin \mathcal{M}_z$. We therefore must additionally backproject $\eta + v$ onto \mathcal{M}_z , by finding a $w \parallel n_\eta$ such that $\eta + v + w \in \mathcal{M}_z$. This can be achieved, for example, by a Newton solver, to solve $F(\eta + v + \alpha n_\eta)$ for $\alpha \in \mathbb{R}$. Crucially, not only does the Newton solver converge to acceptable accuracy extremely quickly, but it also does need only first derivatives of F , which we already know how to compute, and no higher derivatives are required. As discussed in [30], this is in contrast to a possibly more intuitive *orthogonal projection* onto \mathcal{M}_z . This whole procedure is depicted in figure 1.

3.5. Metropolis Hastings adjustment. Now, given a new candidate $\eta + v + \alpha n_\eta = y \in \mathcal{M}_z$, we need to decide whether to accept or reject this proposal point. This is achieved by taking an acceptance probability of

$$\text{accept}(y|\eta) = \min \left(1, \frac{p(y)q(v'|y)}{p(\eta)q(v|\eta)} \right).$$

Here, $p(\eta)$ and $p(y)$ are given by (6) restricted to \mathcal{M}_z (compare appendix A.4), while $q(v|\eta)$ is the probability of drawing the update vector $v \in T_\eta \mathcal{M}_z$ (which we usually choose independent of η), and in reverse, $q(v'|y)$ is the probability to have drawn $v' \in T_y \mathcal{M}_z$ for a step in the opposite direction. For this, note that $v' = \Pi_{T_y \mathcal{M}_z}(\eta - y)$, which necessitates computing the normal vector at y . Of course, if the proposal ends up being accepted, this normal vector can be reused for the next iteration of the algorithm.

It is important to note that on top of the ratio of probabilities of the points, and the ratio of conditional probabilities of the updates, an additional factor must be considered in order to ensure reversibility of the Monte Carlo algorithm: We need to ensure that given y and $v' \in T_y \mathcal{M}_z$, that a Newton search starting from $y + v'$ in direction n_y would end up in the original point η again. If this is not the case, we need to reject the proposal.

Lastly, while the stochastic noise for the original process is drawn from a Gaussian measure on continuous functions (i.e. the Wiener measure), we are actually interested in sampling only from the measure restricted to the submanifold \mathcal{M}_z , so that all samples fulfill the constraint $F(\eta) = z$. Since the manifold \mathcal{M}_z is specified as isoset of the function F , there are geometric considerations to be taken into account as to how the parametrization of F influences the measure restricted to \mathcal{M}_z . As discussed in appendix A.4, this is given by the coarea formula, which assigns to the acceptance probability an additional ratio of volume elements due to the parametrization of \mathcal{M}_z .

3.6. Metropolis Hastings on Hilbert spaces. Even without any constraints, sampling paths of a continuous-time stochastic process such as an SDE implies that we are dealing with infinite dimensional Hilbert spaces. While the above arguments are sound for finite dimensional vector spaces, and one might correctly argue that they therefore also apply to any truncated numerical discretization, it has been noted [21, 37–41] that the naive extension to the functional setup comes with scaling problems if not carefully treated. Concretely, if we choose to discretize the time interval $[0, T]$ with N_t time steps, then the acceptance probability of a Metropolis-Hastings sampler generally approaches zero as $N_t \rightarrow \infty$. The continuum limit $N_t \rightarrow \infty$ in that sense can be viewed as doubly problematic: All computations discussed above, such as the computation of the gradient, or the back-projection onto the manifold, necessitate the solution of differential equations, the cost of which naturally grows when more timesteps are considered. Generally, this is expected to scale linearly with the sample space dimension N_t . In addition to this, we need to consider the number of necessary iterations of the algorithm until it is well-mixed or has sufficiently explored the configuration space, and its scaling with the sample space dimension. It has been realized in [21] and rigorously proven in [42] that in special cases a careful construction of the proposal transition kernel allows the design of Metropolis-Hastings algorithms for which the number of necessary steps in order to reach a given accuracy is *independent* of the sample space dimension. In general, though, the question of scalability of algorithms of the above type is a difficult one. In appendix A, we will briefly summarize results for MCMC on Hilbert spaces, and highlight the associated problems. While these arguments become fairly technical rather quickly, to our knowledge the dimension-independent scaling of MCMC on arbitrary manifolds is an unsolved problem. As we demonstrate in the examples section that follows, though, in many cases of practical interest the disadvantageous scaling is still acceptable and provides usable results, even though the high-dimensional limit poses limitations.

4. EXAMPLES

As examples, we will consider applications from various different areas: First, as demonstration that the algorithm reproduces well-known results, we will sample well-known properties of Brownian bridges in section 4.1. Subsequently, in section 4.2, we will sample a dynamical condensation phase transition as a case of conditioning on a temporal integral. Drawing sample paths realizing a given large stochastic Levy area, as described in

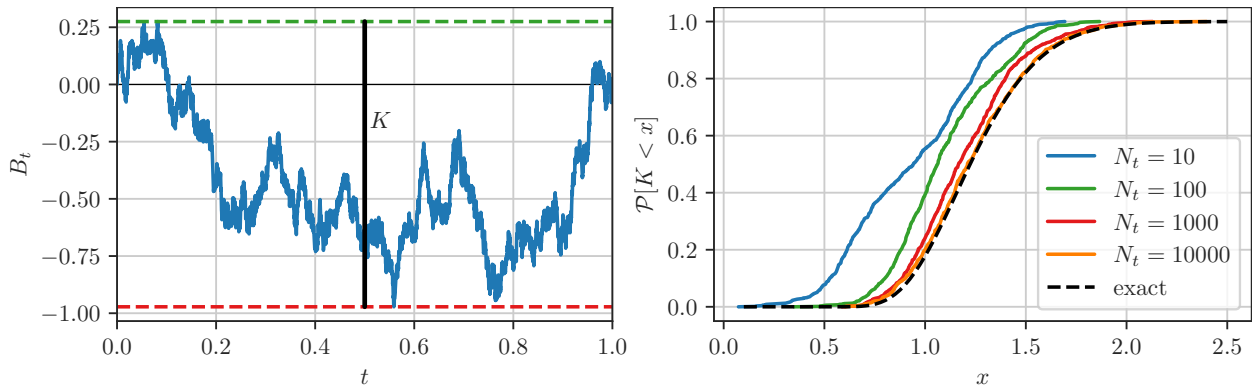


FIGURE 2. Range statistics of the standard Brownian bridge. Left: For a standard Brownian bridge (blue), the range K is given by the difference between its maximal (green) and minimal (red) point. Right: The known statistics of K given by (9) (black dashed) are reproduced by taking empirical statistics over conditioned paths produced by our algorithm (colored lines).

section 4.3 is an example conditioning on a *stochastic* integral. The last two, namely conditioning the Korteweg-deVries equation for shallow water waves on large wave outcomes in section 4.4, and conditioning a model of turbulence in subcritical pipe flow on relaminarization in section 4.5 constitute two examples of stochastically perturbed *partial* differential equation conditioned on an endpoint constraint, demonstrating that the discussed algorithm remains feasible for very large dimensions.

4.1. Range statistics of the standard Brownian bridge. Consider, for 1-dimensional Brownian motion W_t , the standard Brownian bridge B_t given by

$$B_t = W_t - tW_T, \quad B_0 = 0, \quad t \in [0, T], T = 1. \quad (8)$$

While it is not difficult to sample (8), and the above approach is far too general, the Brownian bridge clearly falls into the class of conditioned stochastic differential equations as it can be viewed as a standard Brownian motion conditioned on hitting $W_T = 0$ for $T = 1$. To interpret it in our framework, we set

$$\Phi : L^2([0, 1], \mathbb{R}) \rightarrow L^2([0, 1], \mathbb{R}) \quad \text{with} \quad \Phi : \eta \mapsto \int_0^t \eta(\tau) d\tau$$

that maps noise to trajectory, and as observable take

$$f(\phi) = \phi(T),$$

so that $\mathcal{M}_{z=0} = \{\eta \in L^2([0, 1], \mathbb{R}) \mid \Phi(\eta)(T) = 0\}$ is the constraint manifold corresponding to the standard Brownian bridge. Note that in this case, the adjoint equation (7) is trivially solved by the temporally constant $\mu(t) = z$ and hence the constraint manifold \mathcal{M}_z is a hyperplane and not curved. This simplifies the algorithm significantly, since (i) the tangent space is identical everywhere, (ii) for any $v \in T_x \mathcal{M}_z$ we have that $x + v \in \mathcal{M}_z$ as well, so the projection step is redundant.

The example nevertheless serves as a helpful test case in order to ensure that the algorithm produces correctly conditioned sample paths, both in respect to the scaling limit of taking the number of temporal discretization points to infinity, as well as regarding the statistical properties of the sample paths themselves. As a benchmark test, we want to obtain statistics of the range of the Brownian bridge, defined as the random variable

$$K = \max_{t \in [0, 1]} B_t - \min_{t \in [0, 1]} B_t,$$

i.e. the difference between the highest and lowest point of the standard Brownian bridge (see figure 2 (left)). It is known that the cumulative distribution function of K is given by [43]

$$F_K(x) = \mathcal{P}[K < x] = \sum_{k=-\infty}^{\infty} (1 - 4k^2 x^2) \exp(-2k^2 x^2). \quad (9)$$

Indeed, as visible in figure 2 (right), the correct statistics (9) (black dashed) are reproduced by our algorithm for large N_t . Note in particular how we can freely choose very large N_t without suffering mixing penalties for the high dimension of our sample space if we are using scalable algorithms. Here, we use preconditioned Crank-Nicolson [21] for suggesting a proposal, and consequently the acceptance probability of the Metropolis-Hastings step does not degenerate in the high-dimensional limit.

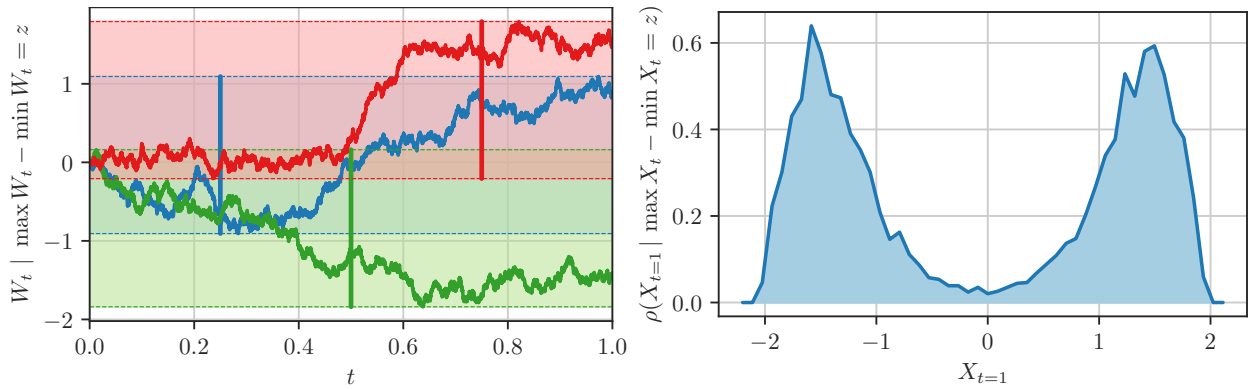


FIGURE 3. Brownian motion conditioned on its range K . Left: Three sample trajectories of Brownian motions W_t such that $\max W_t - \min W_t = z = 2$. The maximal and minimal value of the sample trajectories are indicated by dashed horizontal lines, and the range by a solid vertical line. Right: Endpoints $X_{t=1}$ of the Brownian motion conditioned on a range of $K = 2$ appear to avoid small values and are bimodally concentrated around ± 1.5 .

On the other hand, we are free to look at the exact same problem in reverse: Taking a standard Brownian motion $X_t = W_t$, we can condition on its range

$$K = \max_{t \in [0,1]} X_t - \min_{t \in [0,1]} X_t$$

and instead look at the statistics of the endpoint X_1 , for example the probability distribution function

$$\rho(X_1 | K = z), \quad (10)$$

for which, to the best of our knowledge, no analytical result is known. Note that in this case, \mathcal{M}_z is no longer a hyper-plane, the tangent space non-trivial, and the algorithm no longer simplifies. Results are shown in figure 3, where on the left we demonstrate for three sample trajectories that indeed the range K is always fixed (in this case, we choose $z = 2$), while the right shows the empirical distribution (10) obtained as a histogram over conditioned paths generated by the algorithm. Notably, this distribution as expected is symmetric around 0, and has peaks at approximately ± 1.5 , while avoiding the origin. In other words, a Brownian motion conditioned on a range of $z = 2$ will most likely end away from the origin. We choose $N_t = 10000$.

4.2. Dynamical Condensation Phase Transition in Ornstein-Uhlenbeck process. As a slightly more intricate example, consider the Ornstein-Uhlenbeck process, for $X_t \in \mathbb{R}$, given by

$$dX_t = -X_t dt + \sqrt{\varepsilon} dW_t, \quad X_0 = 0. \quad (11)$$

The invariant distribution of this process is Gaussian, with mean 0 and variance $\varepsilon^2/2$. We now want to condition on the observable

$$f(\phi) = \frac{1}{T} \int_0^T \text{sign}(\phi(t)) |\phi(t)|^\alpha dt, \quad (12)$$

i.e. integrating the process to some power α , keeping track of the sign. In particular, for $\alpha = 1$, this is simply the temporal mean of the process, while higher powers $\alpha > 1$ can be considered as well. It is known [44] that this observable undergoes a condensation phase transition in time with the order parameter α in the following sense: If $\alpha < 2$ then large values of (12) are realized by biasing the linear process (11) to a new mean, and statistics will be Gaussian around the new mean. For $\alpha > 2$, instead, large values of (12) are realized by temporally localized excursions, while the majority of time the process remains Gaussian with mean zero. This is reminiscent of a condensation phase transition in lattice gases, where spatially homogeneous densities transition into localized density spikes, but here with the time variable replacing the spatial extend.

We can probe this phase transition by sampling (11), but conditioned on large values of (12). In figure 4 (left), we see a realization each, for $\alpha = 1.0$ (top) and $\alpha = 3.0$ (bottom), both conditioned on $f(\phi) = z = 0.2$, which for the chosen values of $\varepsilon = 0.1$, $T = 50$, is a rare outlier event. We see that for $\alpha = 1.0$ the event is realized by the whole process shifting to now fluctuate around the new mean 0.2, while for $\alpha = 3.0$ the event is realized by a single, localized excursion (around $t = 37$). The same is visible in the statistics of the process, visualized in figure 4 (right): While the $\alpha = 1.0$ (blue) probability distribution of the conditioned process (shown as markers) remains Gaussian around a new mean (shown as solid line), for $\alpha = 3.0$ (green) the conditioned probability

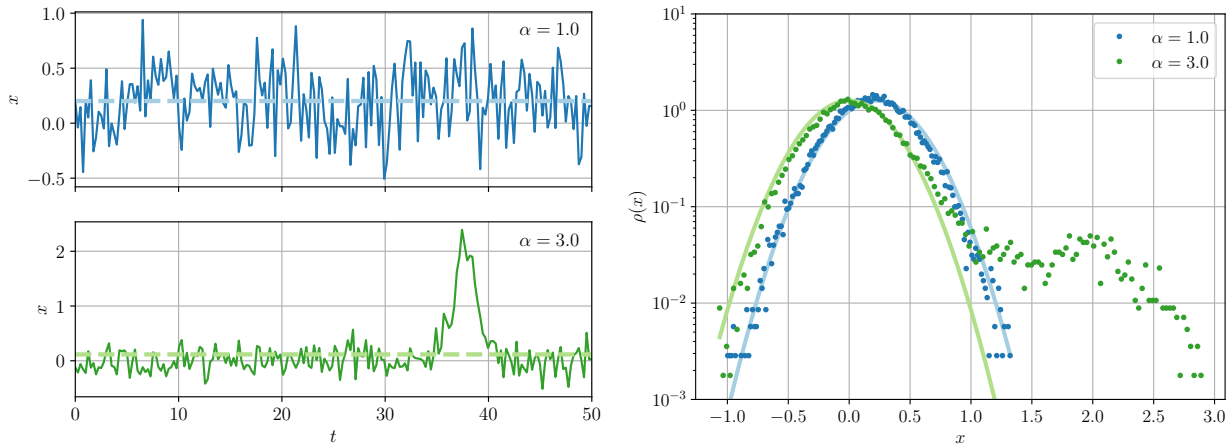


FIGURE 4. Dynamical Condensation Phase Transition. Left: Realizations of the linear process (11) conditioned on large areas (12) for different values of α . For $\alpha = 1$ (top), the large average is realized by shifting the mean. For $\alpha = 3$ (bottom), the large average is realized by a localized excursion (dynamical condensate) instead. Right: The statistics for $\alpha = 1$ (blue), conditioned on large (12), are Gaussian with shifted mean, while for $\alpha = 3$ (green) they have a mean-zero Gaussian core, but with large right tail that contains the dynamical condensate.

distribution (markers) has a mean-zero Gaussian core (solid green line), but an additional heavy tail. We pick $N_t = 200$ time steps here.

4.3. Stochastic Levy area and conditional distributions. The stochastic Levy area [45–50] is defined as the area enclosed by a two-dimensional Brownian motion. More precisely, considering the SDE for $X_t \in \mathbb{R}^2$ given by

$$dX_t = dW_t, \quad X_0 = 0, \quad t \in [0, 1] \quad (13)$$

with $X_t = (X_t^{(1)}, X_t^{(2)})$, the stochastic Levy area is given by

$$A(t, X) = \frac{1}{2} \int_0^t (X_s^{(1)} dX_s^{(2)} - X_s^{(2)} dX_s^{(1)}),$$

which is a stochastic integral in the Ito-sense. We now wish to take as observable the Levy area and condition on a Levy area value of 1, arbitrarily. The algorithm then allows us to draw trajectories from the SDE (13), but always conditioned on the fact that its enclosed area is equal to 1. Figure 5 (left) depicts, in \mathbb{R}^2 , a density of such paths drawn from the algorithm. Since obviously the process is rotation symmetric, here for visualization purposes we choose to rotate all paths such that their endpoint falls onto the x -axis. This allows to visually identify the mechanism by which the path realizes the given area, since all paths lie in a clear tube forming

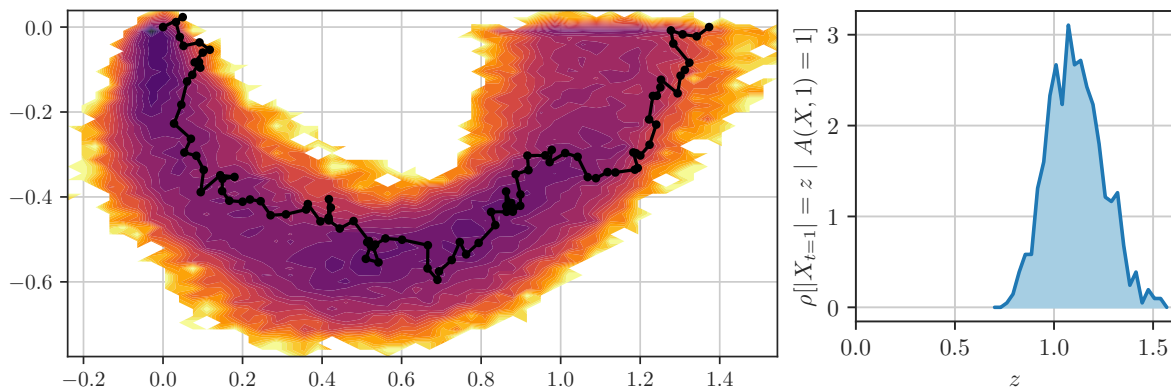


FIGURE 5. Left: path density of two-dimensional Brownian motions conditioned on a Levy area of 1. Here, for visualization purposes, all paths are rotated such that their endpoint is at $X_1^{(2)} = 0$. Right: Conditional probability distribution for the distance of the endpoint from the origin, conditioned on the Levy area being equal to one.

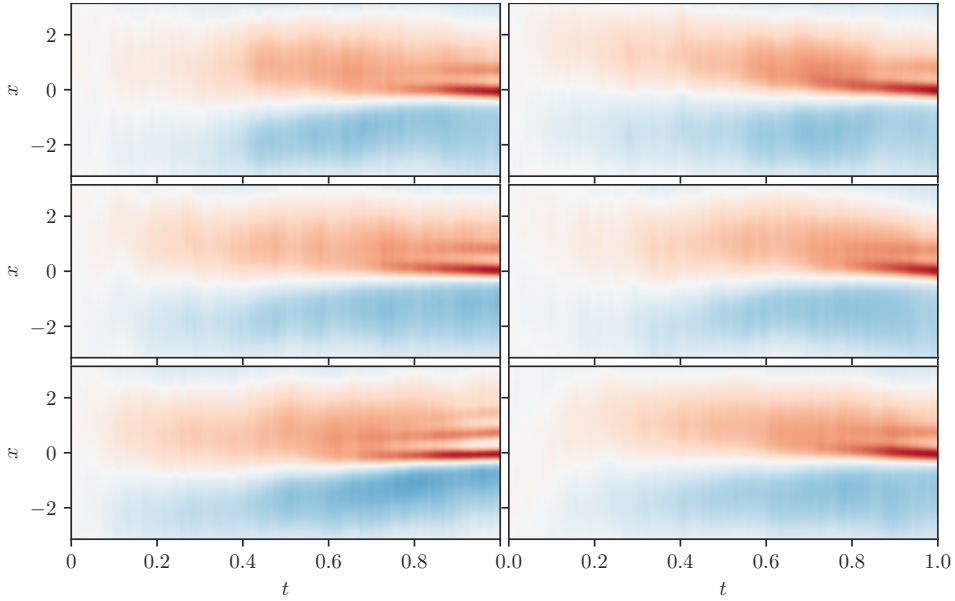


FIGURE 6. Six samples of the stochastic Korteweg-deVries equation (14), conditioned on observing a high wave amplitude at $T = 1$ at the origin $x = 0$. For long times, only random fluctuations in the forced largest scale mode are observed, until the nonlinearity leads to a steepening of the wave and the dispersion then breaks it into multiple wave packets, the largest of which becomes the high wave we condition on. The six samples show that even though all large waves evolve in a similar way, there is considerable variety in their detail such as the number of crests or their movement speed.

roughly a semicircle. In figure 5 (right), we see the conditional probability density of $|X_{t=1}|$ over such paths, namely

$$\rho(|X_{t=1}| > z \mid A(1, X) = 1),$$

i.e. the the probability density of the distance to the origin of the endpoint at $t = 1$, given that the Levy area is equal to 1.

4.4. PDE with endpoint constraint: Stochastic Korteweg-deVries equation. Here, we consider a more complicated example by taking as stochastic PDE the Korteweg-deVries equation for shallow water waves. For an elevation field $\phi(x, t) : [0, L] \times [0, T] \rightarrow \mathbb{R}$, it is given by

$$\partial_t \phi = \kappa \partial_{xxx} \phi + \alpha \partial_{xx} \phi - \phi \partial_x \phi + \eta \quad (14)$$

with dispersion coefficient $\kappa > 0$, diffusion coefficient $\alpha > 0$, and stochastic forcing η , which we take to be long-range correlated in space, white-in-time,

$$\mathbb{E} \eta(x, t) \eta(x', t') = \delta(t - t') \chi(x - x')$$

where in our case $\chi(z)$ only contains the largest-scale Fourier mode contained in the domain (i.e. corresponding to $k = 2\pi/L$).

We are then interested in sampling large waves from a surface at rest at $t = 0$, such that we observe a high wave amplitude at $x = 0$ at $t = T = 1$, corresponding to an observable

$$f(\phi) = \phi(x = 0, t = 1).$$

Since only the largest non-constant mode is stochastically forced, the underlying dimensionality of the sampling problem is not actually higher than that of a low-dimensional SDE, and in fact the noise is $\eta \in L^2([0, T], \mathbb{R}^2)$: Only amplitude and phase of the noise are random (at each instance in time), while its wave number is given. Equivalently, we can view the noise as a complex-valued white-in-time noise. Nevertheless, we need to solve the whole PDE (14) on $[0, T]$ to obtain the surface height at final time at the origin, such that the computation of gradients, both for obtaining the tangent space and for back-projecting onto \mathcal{M}_z , involves deriving through a PDE.

Figure 7 depicts the result of the algorithm, drawing six samples of the stochastic KdV equation (14), conditioned on realizing wave height $z = 5.0$ at $t = T = 1$ at $x = 0$, while all other degrees of freedom are free. The

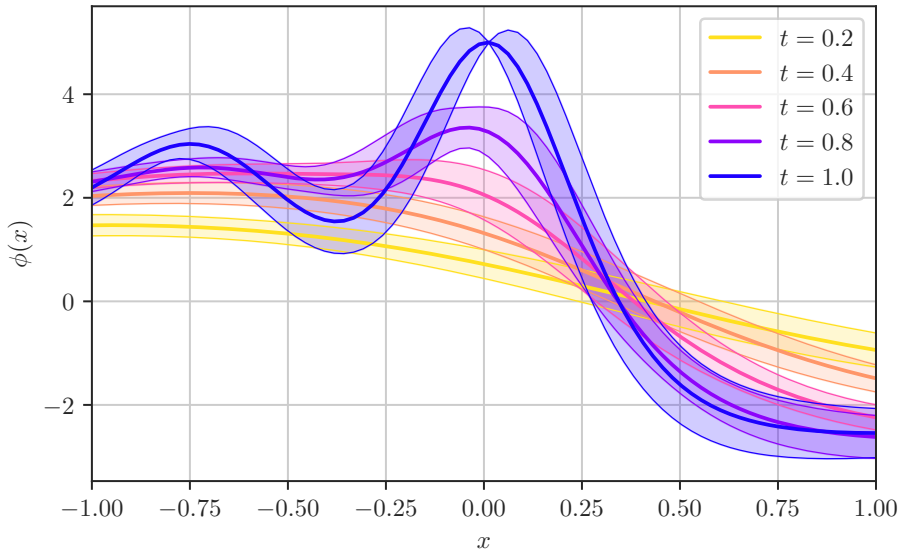


FIGURE 7. Evolution of the Korteweg-deVries equation into a large wave at $t = 1$ at $x = 0$. Here, we choose $z = 5.0$, and plot an ensemble of trajectories that realize this constraint. We additionally plot the standard deviation of all observed realizations.

trajectories are shown in space and time, starting with a flat surface at $t = 0$, and evolving such that a high amplitude wave appears at the origin at final time. There is considerable variety between the samples, concerning e.g. the number of wave crests or the temporal evolution of the zero crossing point.

In figure 7, we show the mean realization over a sampling run, where all samples adhere to the constraint. We additionally show the region of \pm one standard deviation around this mean realization, signifying the possible deviations of observed large waves. The standard deviation must be zero at $x = 0$, since all trajectories fulfill the constraint. Generally, the deviations allow for the wave samples to always look roughly identical, but for example deviate a bit to the left or right.

4.5. Decay of turbulent puffs in subcritical pipe flow. The transition to turbulence in subcritical pipe flow is a classical problem: As first described by Reynolds [51], fluid in a pipe has a transitional regime, where the laminar flow coexists with long-lived turbulent structures, so-called ‘‘puffs’’. With increasing Reynolds number r , puffs become more and more long-lived, but the laminar state remains a linearly stable solution throughout. In this regime, an initially laminar pipe, if left completely undisturbed, remains laminar indefinitely, while a turbulent puff, once excited, is extremely long-lived as well [52].

The ultimate question whether turbulent flow prevails in the pipe is therefore connected to the lifetime of turbulent puffs, and the question of their route to decay back into laminar flow. Since the puffs at intermediate Reynolds numbers are long lived, their decay cannot easily be observed or simulated in this regime, and bespoke rare events algorithms need to be employed [53].

Here, instead, we want to condition the fluid in a pipe to its laminar state in the future, while starting it with a turbulent puff initially. Sampling this process should then generate samples of decaying turbulent puffs, which would otherwise be very rare to observe. To this end, we utilize a stochastic model of turbulent pipe flow introduced by Barkley [54], given by the PDE

$$\begin{cases} \partial_t q + (u - \zeta)\partial_x q = f_r(q, u) + D\partial_x^2 q + \sigma q \eta \\ \partial_t u + u\partial_x u = \epsilon [(U_0 - u) + \kappa(\bar{U} - u)q] \end{cases}, \quad x \in [0, L], t > 0, \quad (15)$$

with $f_r(q, u) = q(r + u - U_0 - (r + \delta)(q - 1)^2)$. Here, x is the direction along the pipe, $u(x, t)$ denotes the mean shear velocity, and $q(x, t)$ quantifies the turbulent velocity fluctuations away from the laminar profile. In other words, $q = 0$ corresponds to laminar flow, while a turbulent puff is a localized region where $q > 0$. Conceptually, this model is a two-species reaction-advection-diffusion equation, but with parameters carefully fitted to the fluid dynamical situation at hand. The parameter r corresponds to the Reynolds number, and η is a spatiotemporal white noise with amplitude σ ,

$$\mathbb{E}\eta(x, t)\eta(x', t') = \delta(t - t')\delta(x - x').$$

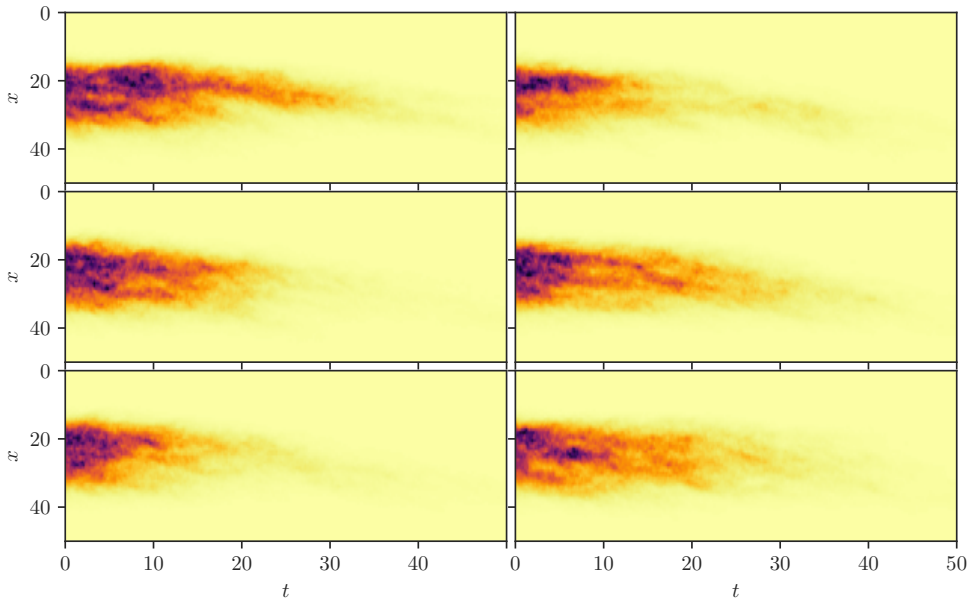


FIGURE 8. Six samples of turbulent puff decay in subcritical pipe flow for the model (15). At initial time, $t = 0$, a turbulent puff is located in the region $x \in [15, 30]$. At the chosen Reynolds number $r = 0.7$, this puff would have an extremely long lifetime of more than 10^4 time units, and observing puff decay would be very difficult. We condition it to instead laminarize by $T = 50$. Depicted is the turbulent velocity component $q(x, t)$ along the decay.

Note that in (15) the stochastic fluctuations are multiplicative Gaussian, since they are proportional to q , which makes physical sense: q signifies chaotic excursions of the Navier-Stokes equations, which are absent for the laminar flow $q = 0$ and become stronger with increasing turbulence.

Equation (15) is a simplified excitable dynamics model of turbulent flow, but agrees with phenomena observed in simulations of the Navier-Stokes equation and experiments to a remarkable degree [54, 55]. From our perspective, though, it is a formidably complicated example: Not only is it a stochastic PDE with white-in-spacetime forcing, but additionally forced degenerately (u has no stochasticity) and multiplicative, with huge portions of the domain where the noise disappears, since $q = 0$ away from the puff. The higher the Reynolds number r , the longer will a turbulent puff survive, so that turbulent puff decay is effectively impossible to observe for high enough r . In particular, expected puff lifetimes τ are hypothesized and experimentally measured to grow doubly exponentially with r , i.e. $\tau \sim \exp(\exp(r))$ [8]. Conditioning the puff onto a decay is therefore a worthwhile endeavor, and getting statistics of puff decay events very difficult to achieve otherwise.

In our simulations, we use the parameters of [54] at a Reynolds number $r = 0.7$ and noise strength $\sigma = 0.25$, with a periodic domain of size $L = 50$. For these parameters, puffs have an expected lifetime of more than 10^4 time units: While the decay event itself happens almost instantaneously on the order of tens of time units, the fluctuations to trigger it are extremely rare, leading to long waiting times in the puff configuration before a decay happens. Concretely, for the application of our algorithm, we define the *turbulent mass* $Q(t)$ via

$$Q(t) = \int_0^L q(x, t) dx,$$

and condition on $Q(T) = 0.1$, i.e. almost vanishing turbulent mass at the final time. For comparison, the turbulent mass of a puff is $Q_{\text{puff}} \approx 25$.

In figure 8, we show six samples of turbulent puff decay in space and time: At $t = 0$, all samples start with a fully developed puff, which then gradually decays as time progresses, to an almost fully relaminarized flow at $T = 50$. In an unconditioned run at this Reynolds number, the expected lifetime of a puff is approximately 10^4 time units and puff decay is very rarely observed. Nevertheless, the decay event itself, once it happens, typically usually evolves from a viable puff into the laminar flow in only tens of time units. Physical features of the decay events depicted in figure 8 qualitatively agree with those of direct stochastic simulations of the system in the literature [9, 54].

5. DISCUSSION

We have introduced an algorithm to sample stochastic (partial) differential equations conditioned on a variety of observables, including endpoint constraints, constraints on nonlinear temporal integrals or even stochastic integrals of the process trajectory. The sampler can be understood as a pathspace Markov chain Monte Carlo algorithm constrained to a manifold. It allows to directly draw from the conditioned path measure, thus also enabling access to conditional distributions of the process, conditioned for example on a rare event. We have demonstrated the applicability of the algorithm to a variety of systems, starting from stochastic processes of academic interest, such as the Brownian bridge or the Levy area, but also considering physically relevant examples, such as dynamical phase transitions, ocean surface waves, or supercritical turbulence in wall-bounded flows. In all cases, we are able to draw from the conditioned path measure, for example to investigate physical causes or typical trajectories for the (often rare) event under consideration.

We remark that a larger number of constraints than a mere scalar variable is possible without much modification. The number of constraints is equal to the co-dimension of the submanifold \mathcal{M}_z , i.e. if $f : \mathbb{R}^n \rightarrow \mathbb{R}^d$, then $z \in \mathbb{R}^d$ and \mathcal{M}_z is co-dimension d . In fact, Zappa *et al.* [30] treat this case as well: The difference is that the projection step now needs to search not for a scalar $\alpha \in \mathbb{R}$ in the Newton solver step above, but for a coefficient vector $\alpha \in \mathbb{R}^d$ to find back to the manifold \mathcal{M}_z . Similarly, projecting onto the tangent space $T_x \mathcal{M}_z$ involves removing d components from an arbitrary proposal vector. Since for systems considered here generally d is much smaller than the dimensionality of the surrounding space (which is technically infinite dimensional, or discretizes to very high dimensions), it is disadvantageous to find an explicit basis for the tangent space, but projection should remain feasible.

Additionally, for acceptable convergence and mixing properties, we rely on the noise-to-observable map F to be sufficiently nice. Clearly, if the encoded differential equation is very sensitive to the stochastic input, local curvature of the manifold \mathcal{M}_z will be very high, necessitating small update steps to obtain non-vanishing acceptance rates in light of the projection step. This might render chaotic systems over long timescales infeasible to be treated. Similarly, the manifold, even if locally relatively weakly curved, might intersect with more likely regions multiple times (or even infinitely many times), leading to a multimodal distribution on the manifold that is hard to sample. The intuition is that a certain observable value might be realizable via multiple discretely different physical mechanisms, and a sampler relying on local updates will remain stuck in local optimum for a long time. This problem is common to many other sampling scenarios and can be alleviated in multiple ways such as replica exchange [56], parallel tempering [57], or metadynamics [29], all of which could be applied to the situation at hand (and in part been [19]).

There are obvious and fundamental questions concerning the rigorous stochastic analysis of the algorithm when considering sampling from infinite dimensional Hilbert spaces. While we address the basics in appendix A, ultimately the problem of dimension-independent scaling of the sampling algorithm is currently unsolved, and we need to resort to statements about the scheme remaining feasible empirically even in the presence of degenerate scaling. These questions of stochastic analysis become even more unbearable when considering SPDEs with white-in-space stochasticity, as we did in section 4.5. Here, there is not even an accepted interpretation of the rigorous meaning of the stated equation (15), where distribution-valued rough fields get freely multiplied in nonlinear terms, without even speaking about conditioning it on nonlinear observables. Nevertheless, the model is widely employed and of practical use in the physical literature (and many others like it in other fields), so that sampling from its finite-dimensional truncation is of value even if the continuum limit will remain nebulous for the foreseeable future.

Acknowledgments. The author wants to thank Timo Schorlepp, Georg Stadler, Jonathan Weare, Alexandros Beskos, Matthew Graham, and Tim Sullivan for helpful discussion.

APPENDIX A. METROPOLIS-HASTINGS ON WIENER SPACE AND CONDITIONAL EXPECTATIONS

A.1. Classical Wiener space. Let $(\mathcal{H}, \langle \cdot, \cdot \rangle)$ be a separable Hilbert space, and induced norm as $\| \cdot \|$. For a positive-definite self-adjoint operator \mathcal{C} , we also define $\langle \cdot, \cdot \rangle_{\mathcal{C}} = \langle \mathcal{C}^{-1/2} \cdot, \mathcal{C}^{-1/2} \cdot \rangle$, with induced norm $\| \cdot \|_{\mathcal{C}}$.

For the construction of the classical Wiener space, we pick $\mathcal{C} = \partial_{tt}^{-1}$ and take \mathcal{H} to be the space of real valued functions $h(t)$ on $[0, T]$ with $h(0) = 0$ such that $\|h\|_{\mathcal{C}} < \infty$. Additionally, we consider the Banach space \mathcal{B} of real valued continuous functions equipped with supremum norm. The classical Wiener measure γ , i.e. the law that defines the process of Brownian motion W_t , is a Gaussian measure on \mathcal{B} with covariance operator \mathcal{C} , and \mathcal{H} is its Cameron-Martin space [58].

Formally, this can be interpreted that the density of γ is given via

$$d\gamma(h) \sim \exp\left(-\frac{1}{2} \int_0^T (\partial_t h(t))^2 dt\right) dh = \exp\left(-\frac{1}{2} \|h\|_{\mathcal{C}}^2\right) dh,$$

with respect to the non-existent Lebesgue-measure dh on \mathcal{B} . While this is only a formal statement, similar statements with respect to a common dominating measures make sense, and are relevant for the formalization of Metropolis-Hastings on Hilbert spaces [59].

A.2. Metropolis-Hastings. Consider now μ a target measure on \mathcal{H} that we want to sample from, its definition relative to the Gaussian measure γ given via $\frac{d\mu}{d\gamma}(x) \propto \exp(-V(x))$ for convenience for a potential V (compare [21, 42]). The idea of the Metropolis-Hastings algorithm is to construct a Markov process on \mathcal{H} with transition kernel $P(x, dy)$ that is reversible with respect to μ , such that drawing from μ is equivalent to sampling the Markov process. Following [59], to construct $P(x, dy)$, we can first consider a Markov chain of our choice with transition kernel $Q(x, dy)$ which we use to generate a proposal. We will accept this proposal with probability $\alpha(x, y)$. This amounts to a transition kernel

$$P(x, dy) = Q(x, dy)\alpha(x, y) + \delta_x(dy) \int (1 - \alpha(x, u))Q(x, du). \quad (16)$$

Here, α needs to be chosen such that $P(x, dy)$ is reversible with respect to μ , i.e. such that the detailed balance condition

$$P(x, dy)\mu(dx) = P(y, dx)\mu(dy) \quad (17)$$

is fulfilled. For that, define $\nu(dx, dy) = \mu(dx)Q(x, dy)$ and $\nu^\perp(dx, dy) = \nu(dy, dx)$. Then, there exists a measurable $R \subset \mathcal{H} \times \mathcal{H}$ such that ν and ν^\perp are equivalent on R (and mutually singular on its complement). We can use this to define $r(x, y) = d\nu|_R/d\nu^\perp|_R(x, y)$ for ν and ν^\perp restricted to R . It can then be shown [59] that the detailed balance condition (17) is fulfilled for the Metropolis-Hastings kernel (16) if we choose

$$\alpha(x, y) = \begin{cases} \min\{1, r(y, x)\} & \text{if } (x, y) \in R \\ 0 & \text{otherwise.} \end{cases} \quad (18)$$

Intuitively, we can interpret $(x, y) \in R$ to mean that $Q(x, dy)$ allows us to reach y from x and vice-versa, and $\alpha(x, y)$ in (18) is chosen precisely such that inserting it into (16) yields (17) on R : the diagonal δ -terms cancel for all α , and (18) fixes the off-diagonal.

A.3. Scaling properties. While in principle the above formalism is correct for any separable Hilbert space, including Wiener space, and generalizes to infinite dimensions, there is a practical problem [42]. Taking for example a proposal distribution $y \sim \mathcal{N}(x, \delta\mathcal{C})$ (which constitutes a standard random walk Metropolis), we have that

$$\frac{d\nu^\perp}{d\nu}(x, y) = \exp\left(-\frac{1}{2} (\|y\|_{\mathcal{C}}^2 - \|x\|_{\mathcal{C}}^2)\right) \exp(V(y) - V(x))$$

independent of δ . Unfortunately, $\|y\|_{\mathcal{C}}$ is almost surely infinite for $y \in \mathcal{B}$, and thus the acceptance probability is zero. While in practice one can argue that all numerical approximations of pathspace quantities will end up finite dimensional, with a discrete number of timesteps N_t , this nevertheless means a broken *scaling* of the algorithm in that $\alpha(x, y) \rightarrow 0$ as $N_t \rightarrow \infty$. As remarked in [21] and rigorously shown in [42], one can circumvent this scaling problem by a suitable choice of proposals (i.e. of $Q(x, dt)$).

To that end, and following [21], we realize that the for a potential $U : \mathcal{H} \rightarrow \mathbb{R}$, the Markov process given by the preconditioned Ornstein-Uhlenbeck process in algorithmic time τ , given by

$$\partial_\tau h_\tau = \mathcal{K}\nabla U(h_\tau) + \sqrt{2\mathcal{K}}\xi_\tau, \quad (19)$$

with \mathcal{K} positive definite preconditioning operator, has an invariant measure proportional to $\exp U(h)$ for any choice of \mathcal{K} , and where ξ_τ is \mathcal{H} -valued white noise in algorithmic time τ . For the case of Gaussian measures with covariance operator \mathcal{C} , we have $U(h) = -\frac{1}{2} \|h\|_{\mathcal{C}}^2$, and hence

$$\partial_\tau h_\tau = -\mathcal{K}\mathcal{C}^{-1}h_\tau + \sqrt{2\mathcal{K}}\xi_\tau, \quad (20)$$

which becomes, for the choice $\mathcal{K} = \mathcal{C}$,

$$\partial_\tau h_\tau = -h_\tau + \sqrt{2\mathcal{C}}\xi_\tau, \quad (21)$$

with $\xi_\tau \sim \gamma$. We can construct a proposal scheme out of this by discretizing the above stochastic differential equation (21) (which is formally an SPDE in the case for infinite dimensional Hilbert spaces). For simplicity,

consider only linear one-step methods to generate a proposal y from the current x , the most general of which is the stochastic θ -method. When solving the SDE $z'(t) = f(z) + \sqrt{2}\xi$, this is given by

$$z_{n+1} = z_n + \theta \delta f(z_{n+1}) + (1 - \theta) \delta f(z_n) + \sqrt{2\delta} \xi_n, \quad (22)$$

and constitutes a convergent integration scheme for any choice of θ (including the explicit and implicit Euler-Maruyama methods for $\theta = 0$ and $\theta = 1$, respectively). We now notice that if we construct $Q(x, dy)$ by discretizing the S(P)DE (21) with the θ -method (22), we obtain

$$Q(x, dy) = \mathcal{L} \left[(1 + \theta\delta)^{-1} \left((1 - (1 - \theta)\delta)x + \sqrt{2\delta C} \xi \right) \right] (dy)$$

for $\xi \sim \gamma$, and where \mathcal{L} denotes the law of its argument. This yields

$$\frac{d\nu^\perp}{d\nu}(x, y) = \exp \left(-\frac{\delta}{4} (2\theta - 1) (\|x\|_C^2 - \|y\|_C^2) \right) \exp(V(y) - V(x)), \quad (23)$$

so that uniquely the choice $\theta = 1/2$ leads to a proposal scheme without any diverging norms. This is the preconditioned Crank-Nicolson scheme (pCN) [21], the first proposal scheme to demonstrate dimension-independent scaling of acceptance rates.

While this approach treats the case of Metropolis-Hastings of target measures on Hilbert spaces relative to a Gaussian reference measure, our situation as presented is considerably more complicated: The additional modification of the acceptance rate by the projection scheme introduces similar ratios of diverging norms. Further, as discussed in section A.4, we need to take into account ratios of curvature terms when considering the restricted Gaussian measure on the manifold. Both these aspects leads to bad scaling properties of the algorithm by Zappa *et al.* [30]. In special cases, such as for example on the sphere [60], these complications can be overcome, and scalable algorithms can be constructed, but to our knowledge the problem remains open in general. For the present work, we restrict ourselves to drawing the proposal via a dimensionally independent pCN step in the case of a flat \mathcal{M}_z without curvature (as in the case of the standard Brownian bridge). In all other cases, we perform the finite-dimensional truncations of all steps involved. This yields acceptable performance for the considered examples, but potentially implies broken dimensional scaling or broken Markovianity (see for example [60, appendix D]).

A.4. Conditional expectations. Unfortunately, it is not our intention to draw from the Wiener measure γ , but instead from a conditional Wiener measure $\eta \sim \gamma|_{F(\eta)=z}$. To make sense of this in terms of Gaussian measures, we first look at the finite-dimensional case, for which there is the well-known coarea formula: Given a measurable function $g : \mathbb{R}^n \rightarrow \mathbb{R}$ and a continuously differentiable function $F : \mathbb{R}^n \rightarrow \mathbb{R}^m$ that foliates \mathbb{R}^n , such that isosets of F are $d = n - m$ dimensional submanifolds of \mathbb{R}^n , we have that

$$\int_{\mathbb{R}^n} g(q) \lambda_n(dq) = \int_{\mathbb{R}^m} \left(\int_{\mathcal{M}_z} g(q) |\det(\nabla F(q)^T \nabla F(q))|^{-1/2} dH_d(q) \right) \lambda_m(dz), \quad (24)$$

where λ_n is the n -dimensional Lebesgue measure, H_d the d -dimensional Hausdorff measure on \mathbb{R}^n , and $\mathcal{M}_z = \{q \in \mathbb{R}^n \mid F(q) = z\} = F^{-1}(\{z\})$ is the preimage of z under F .

The corresponding version for Wiener space, while considerably more technical, can be summarized as follows. For (\mathcal{B}, γ) Wiener space with Cameron-Martin space \mathcal{H} , we are given a map $F : \mathcal{B} \rightarrow \mathbb{R}^d$. This map is said to be “non-degenerate” if the matrix $G_{ij} = \langle DF_i, DF_j \rangle$ is invertible almost surely, and G^{-1} is smooth. Here DF is the element of \mathcal{H} such that $\lim_{\varepsilon \rightarrow 0} \varepsilon^{-1} (f(x + \varepsilon h) - f(x)) = \langle Df, h \rangle$. Then, conditional expectations can be written as

$$\mathbb{E}[g \mid F(\eta) = z] = \int_{\mathcal{M}_z} g(\eta) |\det G(\eta)|^{-1/2} d\gamma_1(\eta),$$

where γ_1 is the Gaussian measure on the co-dimension 1 fiber \mathcal{M}_z [61]. In other words, $|\det G(\eta)|^{-1/2} d\gamma_1(\eta)$ is the disintegration of $d\gamma(\eta)$ on \mathcal{M}_z . This means

$$\gamma(d\eta)|_{F(\eta)=z} = |\det G(\eta)|^{-1/2} d\gamma_1(\eta), \quad (25)$$

which is the actual target measure we want to construct our Metropolis-Hastings algorithm on. Details on the more rigorous statement of these ideas are given in [58, 61, 62].

REFERENCES

- [1] F. Ragone, J. Wouters, and F. Bouchet, Proceedings of the National Academy of Sciences **115**, 24 (2018).
- [2] F. Ragone and F. Bouchet, Geophysical Research Letters **48**, e2020GL091197 (2021).
- [3] J. Lohmann, H. A. Dijkstra, M. Jochum, V. Lucarini, and P. D. Ditlevsen, Science Advances **10**, eadi4253 (2024).
- [4] J. Soons, T. Grafke, and H. A. Dijkstra, Journal of Physical Oceanography (2024), 10.1175/JPO-D-23-0234.1.

- [5] P. Ashwin, S. Wieczorek, R. Vitolo, and P. Cox, *Philosophical Transactions of the Royal Society A: Mathematical, Physical and Engineering Sciences* **370**, 1166 (2012).
- [6] M. Onorato, S. Residori, U. Bortolozzo, A. Montina, and F. T. Arecchi, *Physics Reports Rogue waves and their generating mechanisms in different physical contexts*, **528**, 47 (2013).
- [7] G. Dematteis, T. Grafke, M. Onorato, and E. Vanden-Eijnden, *Physical Review X* **9**, 041057 (2019).
- [8] S. Gomé, L. S. Tuckerman, and D. Barkley, *Philosophical Transactions of the Royal Society A: Mathematical, Physical and Engineering Sciences* **380**, 20210036 (2022).
- [9] A. Frishman and T. Grafke, *Proceedings of the Royal Society A: Mathematical, Physical and Engineering Sciences* **478**, 20220218 (2022).
- [10] Y. Zhang, J. E. Sprittles, and D. A. Lockerby, *Physical Review E* **100**, 023108 (2019).
- [11] J. E. Sprittles, J. Liu, D. A. Lockerby, and T. Grafke, *Physical Review Fluids* **8**, L092001 (2023).
- [12] J. Liu, J. E. Sprittles, and T. Grafke, *Journal of Statistical Mechanics: Theory and Experiment* **2024**, 103206 (2024).
- [13] C.-E. Bréhier, T. Lelièvre, and M. Rousset, *ESAIM: Probability and Statistics* **19**, 361 (2015).
- [14] C. Giardinà, J. Kurchan, V. Lecomte, and J. Tailleur, *Journal of Statistical Physics* **145**, 787 (2011).
- [15] T. Grafke and E. Vanden-Eijnden, *Chaos* **29**, 063118 (2019).
- [16] R. Chetrite and H. Touchette, *Annales Henri Poincaré* **16**, 2005 (2015).
- [17] P. Bolhuis, D. Chandler, C. Dellago, and P. Geissler, *Annual Review of Physical Chemistry* **53**, 291 (2002).
- [18] P. G. Bolhuis and D. W. H. Swenson, *Advanced Theory and Simulations* **4**, 2000237 (2021).
- [19] T. Grafke and A. Laio, *Multiscale Modeling & Simulation* **22**, 125 (2024).
- [20] A. Beskos, G. Roberts, A. Stuart, and J. Voss, *Stochastics and Dynamics* **08**, 319 (2008).
- [21] S. L. Cotter, G. O. Roberts, A. M. Stuart, and D. White, *Statistical Science* **28**, 424 (2013).
- [22] J. Bierkens, F. v. d. Meulen, and M. Schauer, *Advances in Applied Probability* **52**, 173 (2020).
- [23] E. Grong, K. Habermann, and S. Sommer, “Score matching for sub-Riemannian bridge sampling,” (2024).
- [24] P. J. Rossky, J. D. Doll, and H. L. Friedman, *The Journal of Chemical Physics* **69**, 4628 (1978).
- [25] G. O. Roberts and R. L. Tweedie, *Bernoulli* **2**, 341 (1996).
- [26] A. M. Stuart, J. Voss, and P. Wilberg, *Communications in Mathematical Sciences* **2**, 685 (2004).
- [27] M. Hairer, A. M. Stuart, and J. Voss, *The Annals of Applied Probability* **17**, 1657 (2007).
- [28] W. E, W. Q. Ren, and E. Vanden-Eijnden, *Journal of Physical Chemistry B* **109**, 6688 (2005).
- [29] G. Bussi and A. Laio, *Nature Reviews Physics* **2**, 200 (2020).
- [30] E. Zappa, M. Holmes-Cerfon, and J. Goodman, *Communications on Pure and Applied Mathematics* **71**, 2609 (2018).
- [31] M. Girolami and B. Calderhead, *Journal of the Royal Statistical Society: Series B (Statistical Methodology)* **73**, 123 (2011).
- [32] T. Lelièvre, M. Rousset, and G. Stoltz, *Mathematics of Computation* **81**, 2071 (2012).
- [33] T. Lelièvre, M. Rousset, and G. Stoltz, *Numerische Mathematik* **143**, 379 (2019).
- [34] K. Xu and M. Holmes-Cerfon, *Journal of Computational Physics* **506**, 112939 (2024).
- [35] E. Hairer, *BIT Numerical Mathematics* **40**, 726 (2000).
- [36] R.-E. Plessix, *Geophys. J. Int.* **167**, 495 (2006).
- [37] N. Kantas, A. Beskos, and A. Jasra, *SIAM/ASA Journal on Uncertainty Quantification* **2**, 464 (2014).
- [38] T. Cui, K. J. H. Law, and Y. M. Marzouk, *Journal of Computational Physics* **304**, 109 (2016).
- [39] A. Beskos, M. Girolami, S. Lan, P. E. Farrell, and A. M. Stuart, *Journal of Computational Physics* **335**, 327 (2017).
- [40] D. Rudolf and B. Sprungk, *Foundations of Computational Mathematics* **18**, 309 (2018).
- [41] A. Garbuno-Inigo, F. Hoffmann, W. Li, and A. M. Stuart, *SIAM Journal on Applied Dynamical Systems* **19**, 412 (2020).
- [42] M. Hairer, A. M. Stuart, and S. J. Vollmer, *The Annals of Applied Probability* **24**, 2455 (2014).
- [43] M. Perman and J. A. Wellner, *Stochastic Processes and their Applications* **124**, 3106 (2014).
- [44] D. Nickelsen and H. Touchette, *Physical Review Letters* **121**, 090602 (2018).
- [45] M. P. Lévy, *Am. J. Math.* **62**, 487 (1940).
- [46] P. Lévy, in *Proceedings of the Second Berkeley Symposium on Mathematical Statistics and Probability*, Vol. 2 (University of California Press, 1951) pp. 171–188.
- [47] M. Yor, in *Séminaire de Probabilités XIV 1978/79*, Lecture Notes in Mathematics, edited by J. Azéma and M. Yor (Springer, Berlin, Heidelberg, 1980) pp. 343–346.
- [48] N. Ikeda, S. Kusuoka, and S. Manabe, *Stoch. Anal.* **57**, 281 (1995).
- [49] A. Ferreiro-Castilla and F. Utzet, *Stat. Probab. Lett.* **81**, 1380 (2011).
- [50] J. du Buisson, T. D. P. Mnyulwa, and H. Touchette, *Phys. Rev. E* **108**, 044136 (2023).
- [51] O. Reynolds, *Proc. R. Soc.* **35** (1883), 10.1098/rspl.1883.0018.
- [52] K. Avila, D. Moxey, A. de Lozar, M. Avila, D. Barkley, and B. Hof, *Science* **333**, 192 (2011).
- [53] J. Rolland, *Phys. Rev. E* **97**, 023109 (2018).
- [54] D. Barkley, *Journal of Fluid Mechanics* **803** (2016), 10.1017/jfm.2016.465.
- [55] D. Barkley, B. Song, V. Mukund, G. Lemoult, M. Avila, and B. Hof, *Nature* **526**, 550 (2015).
- [56] R. H. Swendsen and J.-S. Wang, *Physical Review Letters* **57**, 2607 (1986).
- [57] E. Marinari and G. Parisi, *Europhysics Letters* **19**, 451 (1992).
- [58] P. Malliavin, *Stochastic Analysis* (Springer, 2015).
- [59] L. Tierney, *The Annals of Applied Probability* **8**, 1 (1998).
- [60] H. C. Lie, D. Rudolf, B. Sprungk, and T. J. Sullivan, *Scandinavian Journal of Statistics* **50**, 1818 (2023).
- [61] H. Airault, P. Malliavin, and J. Ren, *Comptes Rendus. Mathématique* **339**, 637 (2004).
- [62] M. Karmanova, *Journal of Functional Analysis* **254**, 1410 (2008).